

Programmable self-assembly of three-dimensional nanostructures from 10^4 unique components

Luvena L. Ong^{1,2} Nikita Hanikel¹ Omar K. Yaghi¹ Casey Grun¹ Maximilian T. Strauss^{3,4} Patrick Bron⁵ Josephine Lai-Kee-Him⁵ Florian Schueder^{1,3,4} Bei Wang^{1,6} Pengfei Wang⁷ Jocelyn Y. Kishi^{1,8} Cameron A. Myhrvold^{1,8} Allen Zhu¹ Ralf Jungmann^{3,4} Gaetan Bellot*⁹ Yonggang Ke*^{7,10} Peng Yin*^{1,8}

Wyss Institute for Biologically Inspired Engineering, Harvard University, Boston, MA 02115, USA¹

Harvard-MIT Division of Health Sciences and Technology, Massachusetts Institute of Technology,
Cambridge, MA 02139, USA²

Max Planck Institute of Biochemistry, 82152 Martinsried Munich, Germany³

Department of Physics and Center for Nanoscience, Ludwig Maximilian University, 80539 Munich,
Germany⁴

Centre de Biochimie Structurale, CNRS UMR 5048, INSERM U1054, F-34000 Montpellier, France⁵

Department of Polymer Science and Engineering, University of Science and Technology of China, Hefei,
Anhui 230026, China⁶

Department of Biomedical Engineering, Emory University and Georgia Institute of Technology, Atlanta,
GA 30322, USA⁷

Department of Systems Biology, Harvard Medical School, Boston, MA 02115, USA⁸

Institut de Génomique Fonctionnelle, CNRS UMR 5203, INSERM U1191, F-34000 Montpellier, France⁹

Department of Chemistry, Emory University, Atlanta, GA 30322, USA¹⁰

E-mail addresses*: py@hms.harvard.edu, yonggang.ke@emory.edu, gaetan.bellot@igf.cnrs.fr

Nucleic acids (DNA/RNA) are used to construct self-assembled nanoscale architectures with ever increasing complexity.¹⁻¹⁴ Existing DNA nanostructures constructed from one-pot autonomous self-assembly typically contain the order of 10 (e.g. earlier DNA nanostructures^{1,2}) to 10² (e.g. scaffolded DNA origami^{4,6,7,10,13} and DNA brick structures^{8,9}) unique molecular components and have kilo-to mega-dalton scale mass. Here, using a new generation of DNA bricks, we describe 0.1 – 1 gigadalton three-dimensional nanostructures self-assembled from 10⁴ unique components, including a 0.5 gigadalton cuboid containing 30,000 unique bricks, and a 1 gigadalton rotationally symmetric tetramer. A cuboid containing 10,000 bricks was used as a “molecular canvas” with 20,000 uniquely addressable “nano-voxels” to construct structures with sophisticated user-prescribed 3D cavities.

Early DNA nanostructures contained the order of 10 distinct components.^{1,2} A 10-fold increase in component complexity was enabled by scaffolded DNA origami:⁴ in one-pot reaction, the order of 10² components (i.e. ~200 staple strands) self-assemble with an M13 virus scaffold into 2D and 3D structures with 5 megadalton (MDa) mass.^{4,6,7,10,13} Further scaling up of DNA origami^{15,16} via non-hierarchical method will likely need to address the challenge of scaffold manufacturing and routing (especially for sophisticated 3D shapes).

An alternative method to construct complex structures is DNA brick self-assembly,^{8,9} which eliminates the scaffold. Instead, hundreds of short DNA brick strands self-assemble into 2D⁸ and 3D⁹ shapes through specific inter-brick interactions. For the 3D construction, the first generation DNA bricks are 32 nucleotides (nt) long, contain four 8-nt binding domains, and can self-assemble into structures containing the order of 10² distinct bricks. Although DNA brick offers conceptual potential for scaling up, earlier attempts to assemble larger structures encountered practical challenges (e.g. reduced component incorporation rates resulting from low component concentrations, and lowered product formation yields due to competing partial structure formation reactions); experimentally, structures up to 8 MDa were assembled, but with lowered yields and increased portions of unincorporated strands.⁹

Here using a new generation of DNA bricks measuring 52-nt in length, we demonstrate the self-assembly of 0.1 – 1 gigadalton structures from 10⁴ bricks (Fig. 1a, b). Without altering the fundamental design principle of the original 32-nt DNA bricks, the new 52-nt DNA bricks were developed by empirical optimization of the domain dimensions. We investigated structure formation yields by tuning the brick lengths to 52 nt (four 13-nt domains) or 74 nt (two 18-nt and two 19-nt domains), such that the inter-brick binding pattern remains perpendicular. For example, two neighboring 52-nt DNA bricks form a 13-basepair (bp) duplex that corresponds to a 90° inter-brick angle. Comparing 6 helices(H)×6H×8x

base pairs (B), where $x = \{8, 13, 18.5\}$, cuboids assembled from the three different brick types, the 52-nt brick structure showed substantially higher formation yields in both 72-hour thermal annealing (Supplementary Figs. 4, 6, 7, and 8) and isothermal annealing reactions (Supplementary Figs. 5, 11, Supplementary Table 2). Direct comparison of 52-nt brick structures and 32-nt brick structures with similar overall dimensions also revealed that 52-nt brick structures assemble with higher yield and thermal stability (Supplementary Figs. 9 – 12).

Annealing conditions are critical for assembly of 52-nt DNA brick structures. We tested a number of folding conditions, including salinity, temperature ramps, and reaction times, with a 20H×20H×260B structure at a 5 nM strand concentration to obtain an optimal protocol. This 67.6 MDa cuboid had the highest gel yields at ~6% after annealing in 20 mM MgCl₂ isothermally at 51.4°C or using a 1.5°C narrow annealing ramp (52.5 °C to 51°C) over 5 – 7 days (Supplementary Figs. 16, 17).

The scalability of our method was demonstrated by the assembly of seven cuboids of increasing sizes: 10H×10H×156B, 14H×14H×208B, 20H×20H×260B, 30H×30H×260B, 36H×36H×312B, 40H×40H×338B, 46H×46H×390B. These 10.1 to 536 MDa structures were annealed isothermally in one-pot reactions with 20 mM MgCl₂ (Fig. 2a, in grey). An 8H×8H×104B 4.3 MDa origami structure is used as a benchmark (Fig. 2a, b, in blue; Supplementary Figs. 19 – 22). Gel electrophoresis analysis showed 1 – 20% formation yields, depending on the size of the structure and the strand concentration (Fig. 2a, Extended data fig. 1), and revealed an optimal formation temperature range for each structure. In general, as the complexity of the structure increases, the optimal temperature range narrows (Supplementary Fig. 18), suggesting that increased sequence diversity and larger number of components may limit effective nucleation and growth to a smaller window of reaction conditions. Transmission Electron Microscopy (TEM) revealed complete structures with expected dimensions and morphologies using purified samples (Fig. 2, Supplementary Figs. 23 – 46), along with some defective structures (Supplementary Fig. 36) that may reflect incomplete assembly or post-assembly damage during gel purification or TEM sample preparation.

The 46H×46H×390B cuboid was the largest assembled structure (536.4 MDa, over 100 times as massive as an M13scaffolded DNA origami⁴) that is composed of entirely unique components (Fig. 2b, [Supplementary Fig. 43](#)). The cuboid measures over 100 nm in each dimension, contains over 30,000 unique components (33,511 strands) with ~1.7 million nucleotides, and formed with over 1% gel yield. Due to the symmetry present in DNA brick structures, discrete multimer structures can be created by connecting strands across different symmetric planes¹⁷ (Supplementary Figs. 47 – 58). We applied a side-to-side tetramer design to assemble a 1 gigadalton tessellation structure, which measures 72H×72H×312B and contains four identical 262.8 MDa monomeric units (see [Supplementary Figs. 59–61](#) for design

details). Specifically, by utilizing the C4 symmetry¹⁷ present in the plane perpendicular to the DNA helical axis, we designed strands that connected one face of the structure, parallel to the helical axis, to an adjacent face of the same orientation. This connection pattern produced a rotationally symmetric tetramer (Fig. 2c-e, Supplementary Figs. 62 – 64). This gigadalton structure was also formed via simple one-pot isothermal annealing reaction with ~1% gel yield and exhibited designed morphology under TEM (Extended data fig. 1h, Supplementary Figs. 62 – 64, Supplementary Figs. 62, 63). A defect was observed in the center of some particles, possibly due to the putative strain accumulated at the center of the tetramer.

The high component complexity of these cuboids also enables them to be used as programmable “molecular canvases” for complex shape patterning. As a demonstration, we selected the 30H×30H×260B cuboid, which is assembled from 9,700 unique bricks, measures 152 megadalton, and offers 18,000 voxels at a resolution of 13 bp per voxel (Fig. 1c, d). TEM imaging of this cuboid showed that 90% of the particles exhibited expected morphology with no severe distortions (Supplementary Fig. 83), and 3D DNA-PAINT super-resolution imaging^{11,18} further confirmed the expected dimensions for the particles in solution and revealed that all eight corners of most structures are intact (Fig. 2f model, Supplementary Figs. 65, 66).

To facilitate user-friendly design of large 3D brick structures containing the order of 10^4 components, we developed a software tool called *Nanobricks*. First, the user draws, imports, or programs (e.g. via mathematical scripting) a 3D shape by placing “voxels” that represent DNA strand domains. The software then converts the shape into associated DNA brick strands. Finally, the software outputs sequences by generating new or applying an existing set of sequences to the strands (Fig. 3a). The software contains features to add, remove, or modify on the voxel or strand level for each of three steps (Fig. 3a, Supplementary Figs. 67 – 74), and can output file formats compatible with other commonly used DNA structure design and analysis tools¹⁹ (see Supplementary Section S8.4).

We used Nanobricks to design 13 distinct complex cavity shapes from the 30H×30H×260B canvas (Fig. 3, Extended Data Fig. 2, Supplementary Figs. 75 – 83, and Supplementary Table 3). The shapes were designed with one or a combination of three methods: shape importing, mathematical scripting, and manual designing. Nanobrick’s user-friendly 3D visualization and editing interface allowed for easy manipulation of the 18,000 voxels of the molecular canvas (Supplementary Figs. 67 – 74). To determine the minimal feature size, we patterned the surface of a hollow cuboid with varying pore sizes and found that a minimum of 4 helices between separated design features was needed for the structure to form completely (Extended data fig. 2b). Implementing these restrictions, we used the software to convert several open-source 3D designs to voxelized approximations (Figs. 3b, e, f, and Supplementary Fig. 76).

Scripting capabilities allowed for design of complex mathematical cavities, including a helicoid, Möbius strip, hyperboloid, and cone, by identifying whether voxels were located within a given mathematical formula (Figs. 3c, g–i and Supplementary Section S9.4). Manual designs include a structure featuring the projections of “G”, “E”, and “B” along three axes (fig. 3d), one exhibiting the word “LOVE” in one single projection (Figs. 3e), one containing two interconnected loop cavities (Fig. 3j), one with a cavity that threads through itself (Fig. 3k), and other complex shapes (Fig. 3l, m, n).

No “protector strands”⁹ were used within the cavities (Supplementary Fig. 75). Surprisingly, these structures showed strong tolerance to the presence of a large number of exposed “sticky” single-stranded ends inside the cavities, and assembled at yield between 1.5 and 5.1% (Extended data fig. 2c). TEM characterization of the different shapes further showed that approximately 75% of the structures were intact and displayed the expected internal cavities (Supplementary Fig. 83).

Complex structural features were also analyzed in detail by using electron tomography (Fig. 4). We first performed 3D reconstruction on a 30H×30H×260B cuboid with sixteen-parallel 2H×2H×260B crossing channels (Fig. 4a, b). The reconstructions and the 3D visualization using mesh surface representation revealed the 3D channels network in the cuboid. The global topology of the reconstructed density is in agreement with the expected architecture of the object and showed typical shape artifacts at the extreme top and bottom of the particles in the direction of the electron beam due to the missing wedge.²⁰ We then performed electron tomography on four distinct cavity structures: teddy bear, bunny, helicoid, and “GEB” (Fig. 4a-c, e, Supplementary Figs. 86 – 93, and Supplementary Movies). Tilt-series images were collected for each of the three projection views to validate the fine 3D features. Thin features containing only few voxels, such as the teddy bear’s snout and limbs (red arrows in Fig. 4e) or the bunny’s ears (Supplementary Figs. 91 – 93), were confirmed through reconstructions.

To quantitatively examine the incorporation of each of the 10^4 bricks into the structure, we applied a DNA sequencing-based analysis²¹ on the teddy bear structure. The assembled structure was gel purified and heat denatured. The resulting DNA strands were ligated with sequencing primers, amplified, sequenced, and compared with a sample of unreacted strands²¹ (see Supplementary Sections S11.1 and S11.2). Strands with a sequencing read number below a specific threshold are designated as low abundance. By applying this threshold-based analysis to all strands of the molecular canvas, we can extract information about the abundance of each strand in the formed product and thus the average voxel composition of the formed teddy-bear cavity structure (Fig. 5, Supplementary Figs. 104 – 112). Such analysis revealed that the majority (>98%) of the strands forming the teddy bear structure were present in high abundance according to our sequencing analysis (Supplementary Fig. 105), and only a small number of sparsely distributed voxels exhibited undesired low abundance (red voxels in Fig. 5a and

Supplementary Figs. 105 – 106). Projections of the low abundance strands data along the different axes matched the expected projections of the design (Fig. 5b, Supplementary Figs. 111, 112). By normalizing the data, we observed a “hot spot” of low-abundance strands at the back of the teddy bear, which is consistent with some broken particles observed by TEM (Supplementary Fig. 112). This structural defect could potentially be caused by the presence of only a few crossovers at this tenuous spot.

We have constructed DNA nanostructures from 10^4 unique components, with molecular weights up to the gigadalton scale. The 0.5 GDa structure contains 33,511 unique components, 1,684,336 nt of sequence, and bridges two orders of magnitude in length in all three dimensions in a space filling fashion: from a feature resolution of $2.8 \times 2.8 \times 4.4 \text{ nm}^3$ to assembled structures with an 100 nm length in each of the three dimensions. The work here focuses on constructing compact, spacing filling structures, and packed 10^4 unique components in 1 attolitre (i.e. $100 \times 100 \times 100 \text{ nm}^3 = 10^{-21} \text{ m}^3$) space. It should also be feasible to use variations of the bricks to construct wire-frame or porous structures^{10,11,13,14} with similar component complexity.

In 2006, DNA origami’s 10-fold leap in component complexity ushered in diverse applications, e.g. in single molecule biophysics,²² structural biology,²³ synthetic biology,²⁴ nanofabrication,^{25,26} and photonics.²⁷ The new 100-fold increase in complexity by DNA bricks will likely enable additional functionality (e.g. as scaffolds for patterning complex inorganic nanostructures²⁵ or for 3D positioning of diverse functional moieties^{26,27}).

The 52-nt bricks appeared capable of mitigating reduced kinetics associated with unavoidable decreased component concentration in assembly of large DNA structures with a massive number of distinct components. While the detailed mechanism of brick structure formation remains to be experimentally dissected, our results here are consistent with the hypothesized assembly mechanism of delayed nucleation followed by fast growth.^{9,28} When domains were increased from 8-nt to 13-nt, the structures were observed to form more rapidly. Additionally, researchers have found that binding heterogeneity circumvents the emergence of multiple dominant competing nuclei.²⁸ The component heterogeneity is further enhanced in our 52-nt brick design because the range of accessible binding energies becomes wider with longer domains due to the larger sequence space.

The high cost of purchasing a large number of synthetic DNA strands logically restricted our testing to ~30,000 distinct bricks in this study. Low-cost methods for synthesizing DNA strands (e.g. chip-synthesized DNA followed by parallel enzymatic amplification²⁹) may enable investigation into even larger assembly with DNA bricks in future. Alternatively, scaling-up could also be achieved by hierarchical methods via sticky end association or shape complementarity.^{12,30}

References

1. Chen, J. & Seeman, N. C. The synthesis from DNA of a molecule with the connectivity of a cube. *Nature* **350**, 631–633 (1991).
2. Winfree, E., Liu, F., Wenzler, L.A. & Seeman, N.C. Design and self-assembly of two-dimensional DNA crystals. *Nature* **394**, 539–544 (1998).
3. Shih, W.M., Quispe, J.D. & Joyce, G.F. A 1.7-kilobase single-stranded DNA that folds into a nanoscale octahedron. *Nature* **427**, 618–621 (2004).
4. Rothemund, P.W.K. Folding DNA to create nanoscale shapes and patterns. *Nature* **440**, 297–302 (2006).
5. Zheng, J. P. *et al.* From molecular to macroscopic via the rational design of a self-assembled 3D DNA crystal. *Nature* **461**, 74–77 (2009).
6. Douglas, S. M. *et al.* Self-assembly of DNA into nanoscale three-dimensional shapes. *Nature* **459**, 414–418 (2009).
7. Han, D. *et al.* DNA origami with complex curvatures in three-dimensional space. *Science* **332**, 342–346 (2011).
8. Wei, B., Dai, M. & Yin, P. Complex shapes self-assembled from single-stranded DNA tiles. *Nature* **485**, 623–626 (2012).
9. Ke, Y., Ong, L. L., Shih, W. M. & Yin, P. Three-dimensional structures self-assembled from DNA bricks. *Science* **338**, 1177–1183 (2012).
10. Han, D. *et al.* DNA gridiron nanostructures based on four-arm junctions. *Science* **339**, 1412–1415 (2013).
11. Iinuma, R. *et al.* Polyhedra self-assembled from DNA tripods and characterized with 3D DNA-PAINT. *Science* **344**, 65–69 (2014).
12. Gerling, T., Wagenbauer, K.F., Neuner, A.M. & Dietz, H. Dynamic DNA devices and assemblies formed by shape-complementary, non-base pairing 3D components. *Science* **347**, 1446–1452 (2015).
13. Benson, E. *et al.* DNA rendering of polyhedral meshes at the nanoscale. *Nature* **523**, 441–444 (2015).
14. Veneziano, R. *et al.* Designer nanoscale DNA assemblies programmed from the top down. *Science* **352**, 1534 (2016).
15. Marchi, A.N., Saaem, I., Vogen, B.N., Brown, S. & Labean, T.H. Towards larger DNA origami. *Nano Letters* **14**, 5740–5747 (2014).
16. Nickels, P.C. *et al.* DNA origami structures directly assembled from intact bacteriophages. *Small* **10**, 1765–1769 (2014).

17. Liu, Y., Ke, Y. & Yan, H. Self-assembly of symmetric finite-size DNA nanoarrays. *J. Am. Chem. Soc.* **127**, 17140–17141 (2005).
18. Jungmann, R. *et al.* Multiplexed 3D cellular super-resolution imaging with DNA-PAINT and Exchange-PAINT. *Nature Methods* **11**, 313–318 (2014).
19. Douglas, Shawn M *et al.* Rapid prototyping of 3D DNA-origami shapes with caDNAno. *Nucleic Acids Research* **37**, 5001–5006 (2009).
20. Weyland, M. & Midgley, P.A. 3D electron microscopy in the physical sciences: the development of Z-contrast and EFTEM tomography. *Ultramicroscopy* **96**, 413–431 (2003).
21. Myhrvold, C. *et al.* Barcode extension for analysis and reconstruction of structures (BEARS). *Nature Communications* **8**, 14698 (2017).
22. Nickels, P. C. *et al.* Molecular force spectroscopy with a DNA origami– based nanoscopic force clamp. *Science* **354**, 305–307 (2016).
23. Douglas, S. M., Chou, J. J. & Shih, W. M. DNA-nanotube-induced alignment of membrane proteins for NMR structure determination. *Proc. Natl Acad. Sci. USA* **104**, 6644–6648 (2007).
24. Fu, J. *et al.* Multi-enzyme complexes on DNA scaffolds capable of substrate channeling with an artificial swinging arm. *Nature Nanotechnology* **9**, 531–536 (2014).
25. Sun, W. *et al.* Casting inorganic structures with DNA molds. *Science* **346** (2014).
26. Knudsen, J. B. *et al.* Routing of individual polymers in designed patterns. *Nature Nanotechnology* **10**, 892–898 (2015).
27. Acuna, G P *et al.* Fluorescence enhancement at docking sites of DNA-directed self-assembled nanoantennas. *Science* **338**, 506–510 (2012).
28. Jacobs, W.M., Reinhardt, A. & Frenkel, D. Rational design of self-assembled pathways for complex multicomponent structures. *Proc. Natl. Acad. Sci. USA* **112**, 63136318 (2015).
29. Schmidt, T.L. *et al.* Scalable amplification of strand subsets from chip-synthesized oligonucleotide libraries. *Nature Communications* **6**, 8634 (2015).
30. Rajendran, A., Endo, M., Katsuda, Y., Hidaka, K. & Sugiyama, H. Programmed Two-Dimensional Self-Assembly of Multiple DNA Origami Jigsaw Pieces. *ACS Nano* **5**, 665–671 (2011).

Acknowledgments: The authors thank N. Ponnuswamy, R. Sørensen, J. Hahn, J. Lara, L. Chou, N. Garreau, S. Saka, H. Sasaki, J.B. Woehrstein, and C.B. Marks for experimental help. The authors also thank B. Wei, W. Sun, and W.M. Shih for insightful discussions, M. Beatty and J. Cheng for help in developing the Nanobricks platform, and C. Chen for assistance with draft preparation. The work was funded by Office of Naval Research grants N000141010827, N000141310593, and N000141410610, an Army Research Office grant W911NF1210238 (P.Y.); An Emory Biomedical Engineering Department Startup Fund, an Emory Winship Cancer Institute Billi and Bernie Marcus Research Award, an Winship Cancer Institute grant #IRG-14-188-0 from the American Cancer Society, an National Science Foundation CAREER Award DMR-1654485 (Y.K.); French National Research Agency grants ANR-16-CE09-0004-01, ANR-15-CE09-0003-02 (G.B.); an French National Research Agency grant ANR-10-INBS-05 (P.B.). L.L.O. was funded by an NSF graduate research fellowship. N.H. was funded by the German National Academic Foundation and German Academic Exchange Service. M.T.S. acknowledges support from the International Max Planck Research School for Molecular and Cellular Life Sciences (IMPRS-LS).

Author contributions: L.L.O. conceived the project, designed and performed the experiments, analyzed the data, and wrote the paper. N.H. designed and performed the experiments, analyzed the data, and wrote the paper; O.K.Y., B.W. and P.W. performed the experiments and analyzed the data. M.T.S. and F.S. performed the 3D DNA-PAINT experiments, analyzed the data, and wrote the paper. C.G. and J.Y.K. developed the Nanobricks software and wrote the paper. P.B. and J.L. performed the electron tomography experiments. C.A.M. designed and analyzed the sequencing experiments and wrote the paper. A.Z. performed the experiments. R.J. supervised the DNA-PAINT experiments, interpreted data, and wrote the paper. G.B. designed and supervised the electron tomography study, interpreted data, and wrote the paper. Y.K. and P.Y. conceived, designed, and supervised the study, interpreted the data, and wrote the paper.

Competing financial interests: A patent has been filed based on this work. P.Y. is co-founder of Ultivue Inc. and NuProbe Global.

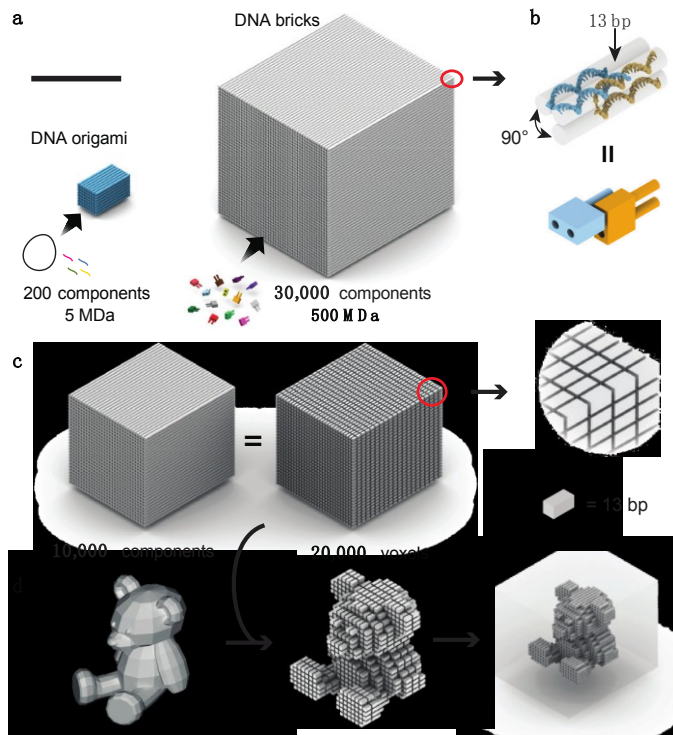


Figure 1:Three dimensional nanostructures self-assembled from DNA bricks. **a**, Comparison of 3D DNA origami (~200 components, ~5 megadalton),⁴ and DNA brick nanostructures assembled here (~30,000 unique components, ~500 megadalton). **b**, Detailed helical (top) and brick (bottom) models of incorporated 52-nt DNA brick strands. **c**, A ~150 MDa DNA brick cuboid (left) as a molecular canvas (middle) composed of ~20,000 13-bp voxels (right). Scale bar in **a** and **c** measures 100 nm. **d**, A 3D teddy bear rendering (left) can be approximated using the ~20,000 voxel canvas (middle) to form the cavity of a cuboid structure (right).

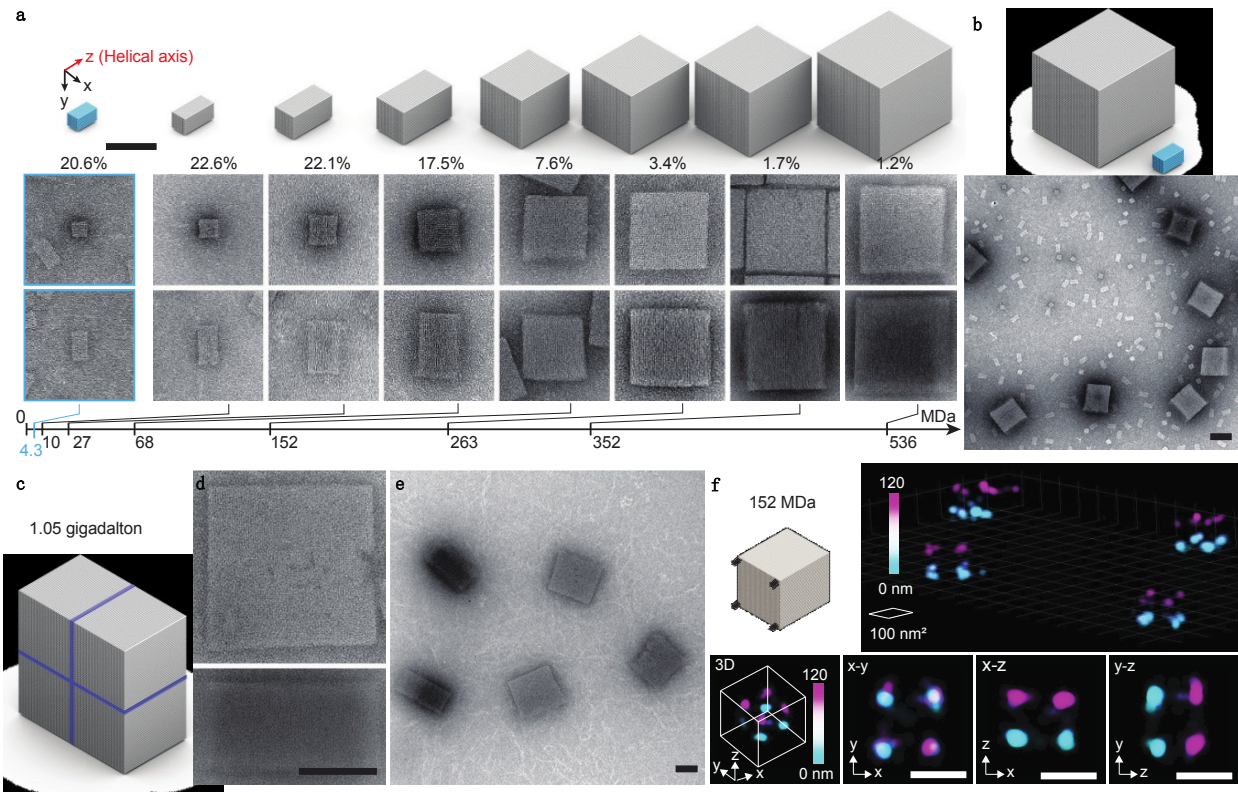


Figure 2: Self-assembly of brick cuboids. Cylindrical models of DNA brick cuboids (gray) and an M13-scaffolded DNA origami cuboid (blue). **a**, Comparison of gel yields (top numbers), TEM images of helical end view (middle), and lateral projection (bottom) of DNA cuboids. **b**, Model (top) and TEM image (bottom) of 536 MDa brick cuboids and 4.3 MDa origami cuboids. 1.05 gigadalton cuboid model (**c**), selected TEM helical (top) and lateral (bottom) images (**d**), and wide-field TEM images (**e**). **f**, 3D DNA-PAINT super-resolution images of the 152 MDa canvas structure: a wide-field view (top) and different projections of a single representative cuboid (bottom). Color bars indicate height along the *z*-axis. All scale bars measure 100 nm.

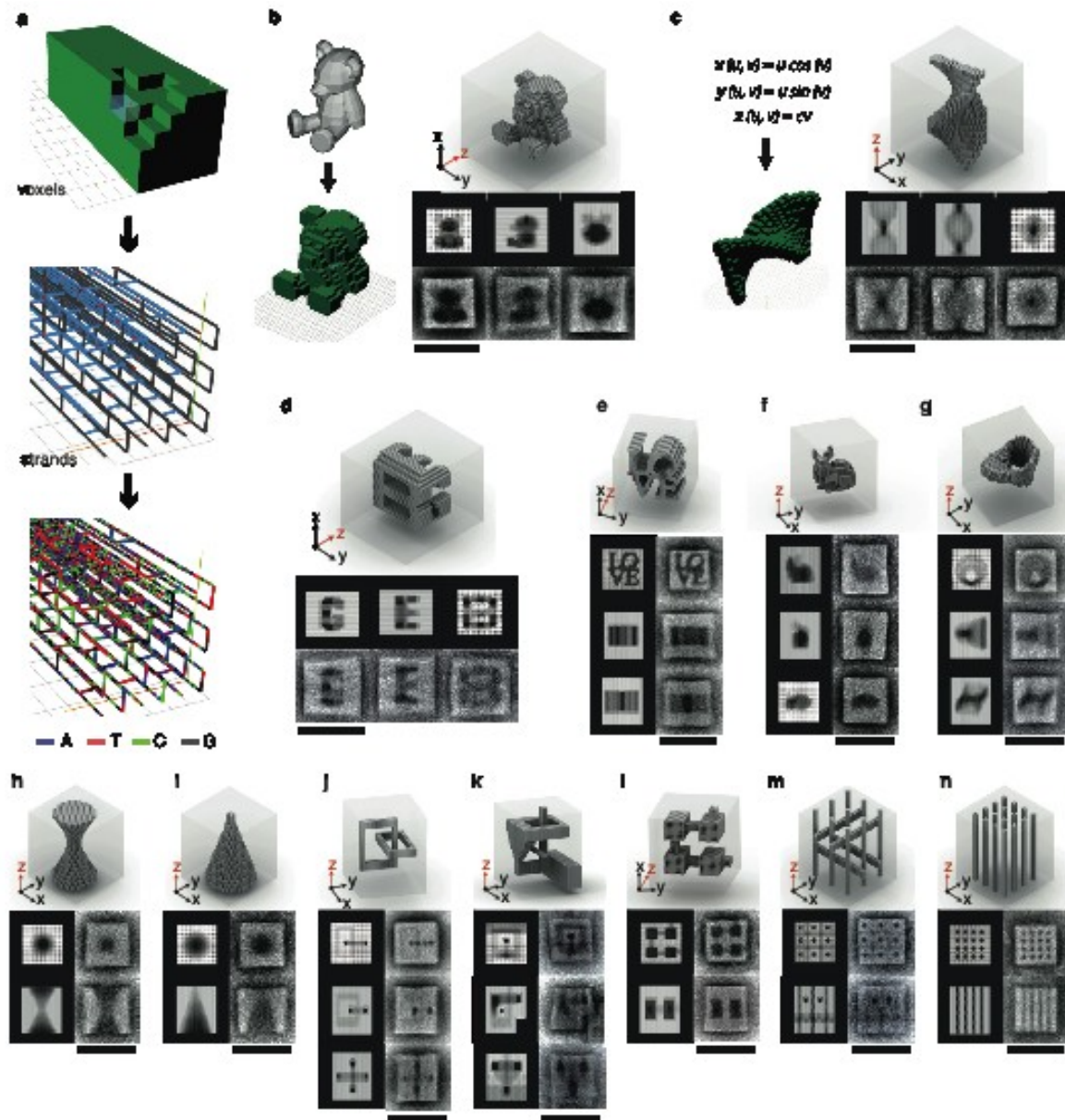


Figure 3: Cavity shapes formed from a $30H \times 30H \times 260B$ molecular canvas. **a**, Design software for complex DNA brick structures. Desired shapes can be designed by editing voxels through a 3D interface (top), translated automatically to strands (middle), and assigned sequences (bottom). **(b, c)** Cavity shapes can be generated by selecting or excluding (right) voxels to approximate 3D rendering files **(b)** or to satisfy mathematical equations **(c)**. **(d - n)** Diverse cavity shapes. For each design, the top diagram depicts a 3D model of the designed shape. Expected projections (top or left) and averaged TEM images (bottom or right) are also shown. Individual particles used in averaged images are depicted in Supplementary Table 3 and Supplementary Figs. 77 – 82. Scale bars measure 100 nm.

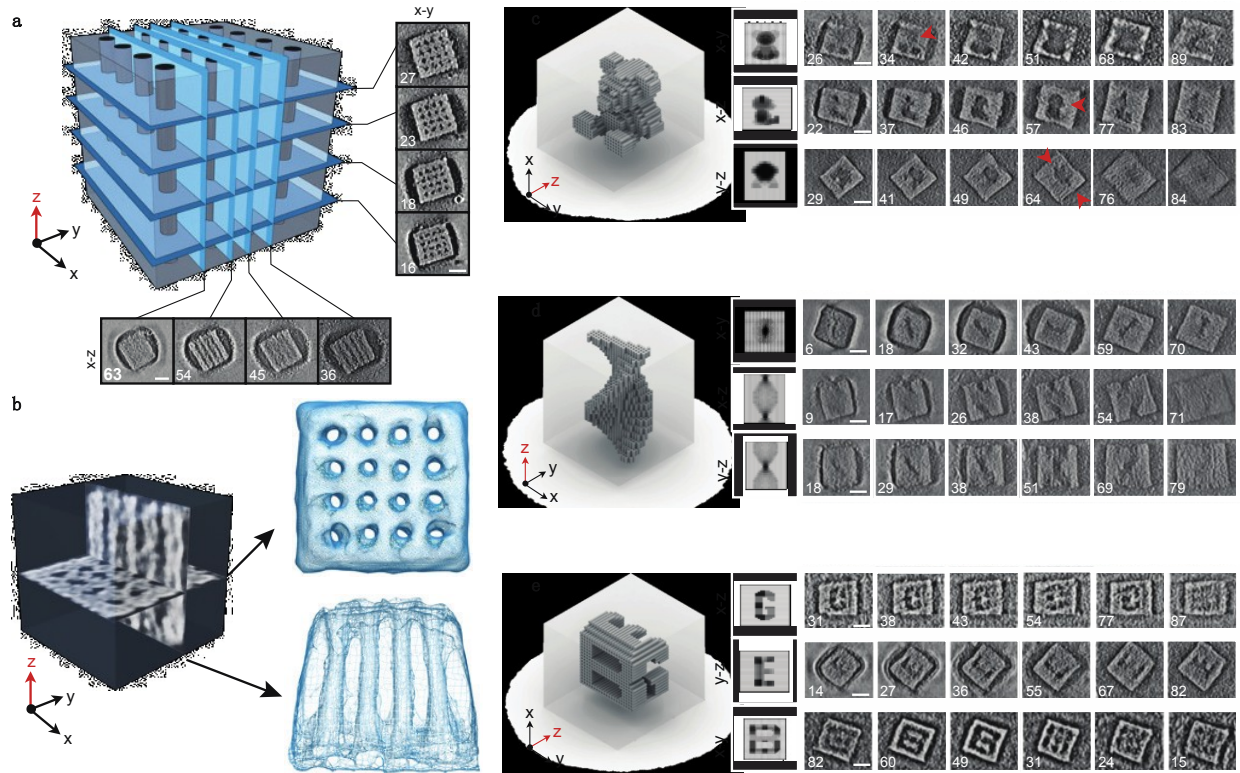


Figure 4: Electron tomography analysis and computational 3D reconstruction of DNA brick structures. **a**, 3D model of a cuboid containing parallel channels, with extracted slices from the tomogram (right and bottom). **b**, 3D model of the cuboid in a showing the positions of two orthogonal slices (left), and the corresponding 3D mesh-rendered view of their tomographic reconstructions (right). **(c -e)**, 3D model (left), expected shape projections (middle), and slices extracted from tomograms (right) for the teddy bear **(c)**, helicoid **(d)**, and “GEB” **(e)** structures. Red arrows point to thin but visible features. Numbers in images correspond to slice position extracted from each tomogram (see Supplementary Figs. 84 – 93 and Supplementary Movies for more details). All scale bars measure 50 nm.

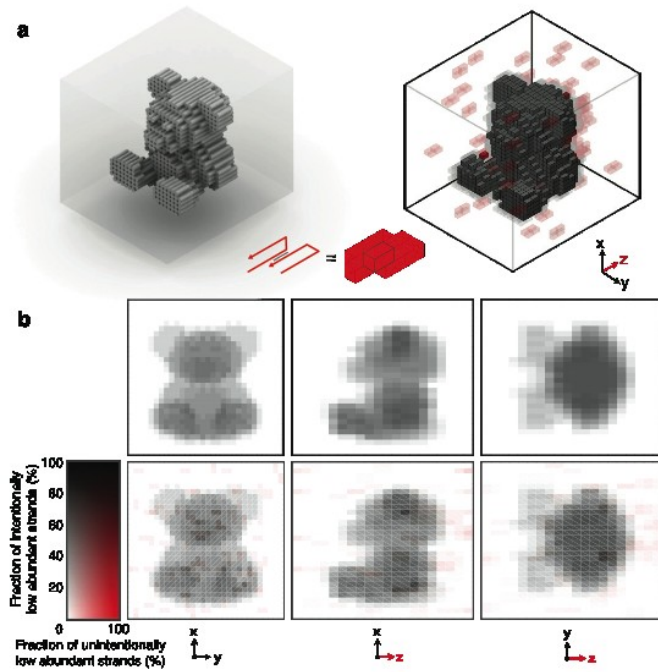


Figure 5: DNA sequencing analysis of the teddy bear city structure. **a**, 3D model (left) and 3D representation of sequencing results (right) of the teddy bear design. Gray and red colors correspond to intended (in cavity) and unintended (in structure) low abundance species, respectively. Opacity of voxels corresponds to the number of strands for which a criterion applies: completely opaque – two, partially transparent – one. Voxels formed by two well incorporated strands are not depicted. **b**, Schematic 2D representations (top) and respective 2D plots of the fractions of low abundance strands along a given axis (bottom).

Methods

Condensed descriptions of methods are described below. See the Methods section in the Supplementary Information for specific details.

Design and formation of structures. Structures were designed using our Nanobricks software. Depicted 2D strand diagrams were generated from associating caDNAno files.¹⁹ Structures were annealed in 0.5×TE buffer (5 mM Tris, 1 mM EDTA, pH 8) containing 20 mM MgCl₂ using either an isothermal hold³¹ or a narrow annealing ramp. See Supplementary Methods and Supplementary Table 1 for the detailed annealing conditions and optimal temperatures. [See supplementary information for sequences used for each structure.](#)

Agarose gel electrophoresis. Samples were analyzed using 0.3-2% agarose gel electrophoresis and stained using SYBR Safe loading dye. Gels were visualized using the Typhoon FLA 9000 gel imager and quantified using ImageJ³² or TotalLabQuant v12.2 (Cleaver Scientific, ltd).

Transmission electron microscopy imaging. Samples were deposited on glow-discharged formvar/carbon coated grids from Electron Microscopy Sciences. Samples were stained for 60 seconds with 2% uranyl formate solution containing 25 mM NaOH and imaged using a JEOL JEM-1400 TEM operated at 80 kV.

Electron tomography and image processing. Samples were deposited on glow-discharged, carbon-coated 300 mesh copper grids and stained using 1% uranyl acetate solution. The grids were then transferred into a JEOL 2200FS FEG transmission microscope using the JEOL high tilt holder. Series of tilted images were collected at a magnification of 50,000 folds by using a 4k × 4k slow-scan CCD camera (Gatan, inc.) with defocus values of -3 μm and -5 μm. The acquisition was performed semi-automatically using the Serial EM software package. Samples were tilted between -60° and 60° with 2° increment steps. For a detailed description of the alignment and reconstruction procedure see the Supporting Information.

3D DNA-PAINT super-resolution setup. Fluorescence imaging was [performed using an](#) inverted Nikon Eclipse Ti-E microscope (Nikon Instruments, Melville, NY) with the Perfect Focus System, applying an objective-type TIRF configuration with an oil-immersion objective (CFI Apo TIRF 100×, NA 1.49, Oil). 3D images were acquired using a cylindrical lens (FL = 1m) in the detection path.

Super-resolution DNA-PAINT images were reconstructed using spot-finding and 2D-Gaussian fitting

algorithms programmed in LabVIEW.¹⁸ A previously published calibration function³³ was used for 3D calibration. Drift correction was performed on the DNA structures, as previously described.³⁴

Z-calibration was additionally corrected for refractive-index-mismatch by measuring a reference structure with given height, resulting in a correction factor of 1.3.¹¹ ViSP³⁵ was used to visualize single-particle localizations in three dimensions. After exporting from ViSP, images and corresponding color bars were contrast-adjusted using Fiji.³⁶ See the Supplementary Methods for additional details on sample preparation and image analysis.

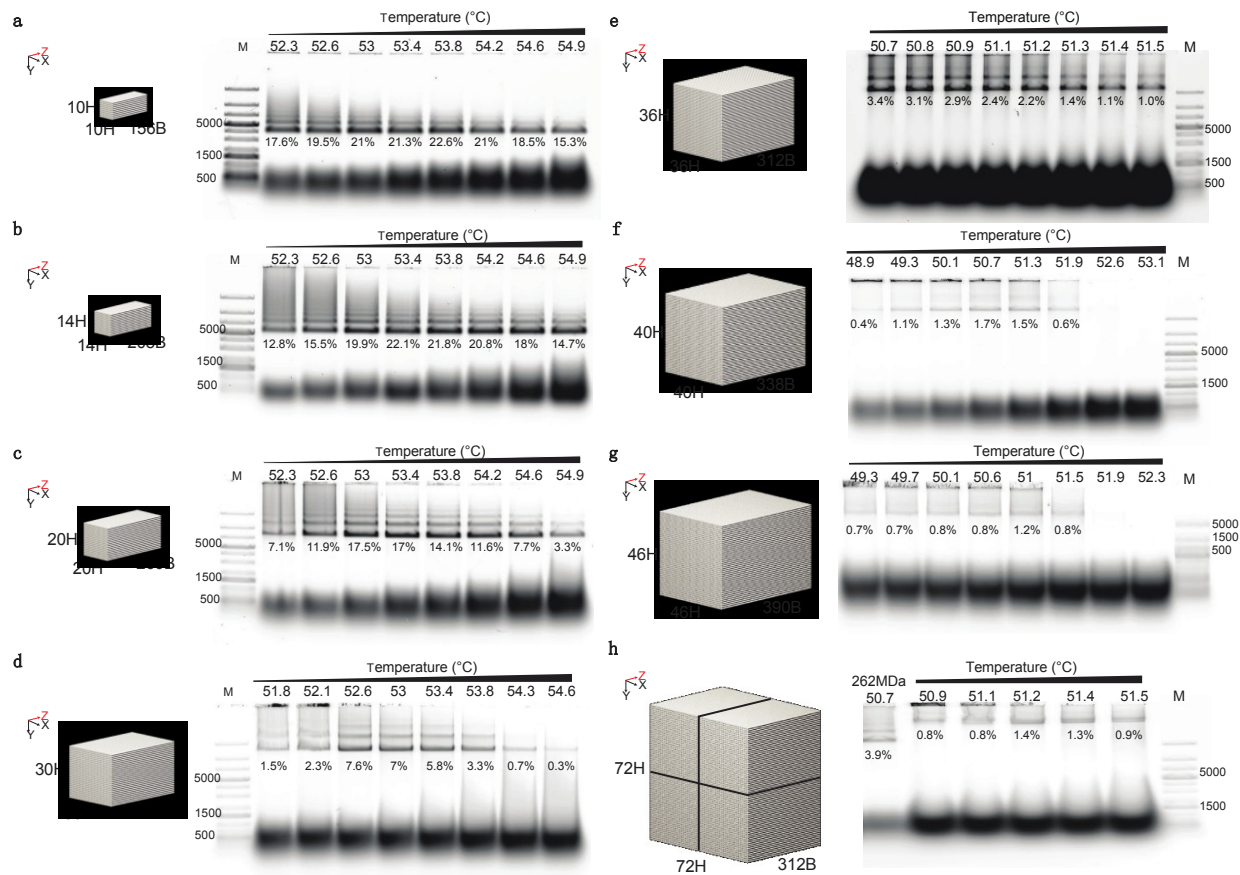
Sequencing sample preparation and analysis. Sequencing analysis was prepared following a modified version of the barcode extension for analysis and reconstruction of structures (BEARS) protocol.²¹ Samples were ligated to an adaptor sequence on the 5' end using T4 RNA ligase 1 (New England Biolabs) and purified using polyacrylamide gel electrophoresis and electroelution. Subsequently, the 3' end of the strands was ligated to a previously tested adaptor sequence²¹ containing an integrated barcode. Then samples were amplified using Q5 polymerase.

Multiple samples with different barcodes were pooled and sequenced with an Illumina MiSeq machine according to the manufacturer's instructions by using the MiSeq V2 paired end 50 kit (Illumina Inc., San Diego, CA). A modified library denaturation and loading protocol for lower concentration libraries was used.³⁷

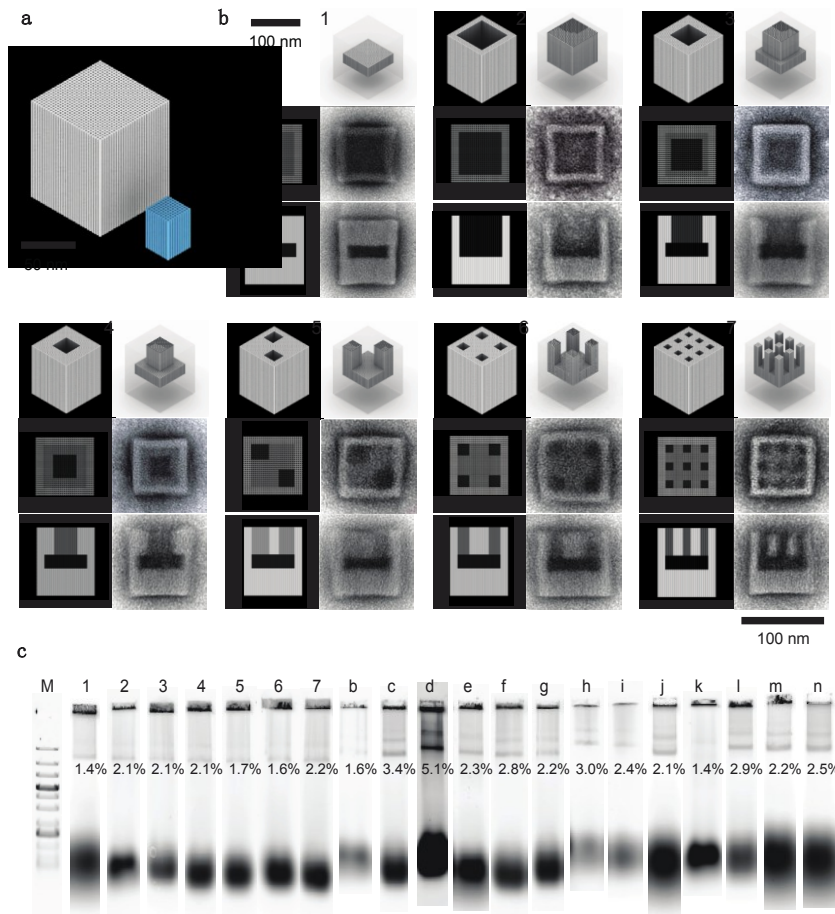
Data availability. The authors declare that the main data supporting the findings of this study are available within the paper and its Supplementary Information files. Sequences used to form the large structures are provided as well. Structure designs and software are posted at <https://yin.hms.harvard.edu/bricks/try/#>. All other data supporting the findings of this study are available from the corresponding authors on request.

References

31. Sobczak, Jean-Philippe J, Martin, Thomas G, Gerling, Thomas & Dietz, Hendrik. Rapid folding of DNA into nanoscale shapes at constant temperature. *Science* **338**, 1458–1461 (2012).
32. Schneider, C.A., Rasband, W.S. & Eliceiri, K.W. NIHImage to ImageJ: 25 years of image analysis. *Nature Methods* **9**, 671–675 (2012).
33. Huang, B., Wang, W., Bates, M. & Zhuang, X. Three-dimensional super-resolution imaging by stochastic optical reconstruction microscopy. *Science* **319**, 810–813 (2008).
34. Lin, C. *et al.* Sub-micrometer geometrically encoded fluorescent barcodes self-assembled from DNA. *Nature Chemistry* **4**, 832–839 (2012).
35. El Beheiry, M. & Dahan, M. ViSP: representing single-particle localizations in three dimensions. *Nature Methods* **10**, 689–690 (2013).
36. Schindelin, J. *et al.* Fiji: an open-source platform for biological-image analysis. *Nature Methods* **9**, 676–682 (2012).
37. Quail, M.A. *et al.* A large genome center's improvements to the Illumina sequencing system. *Nature Methods* **5**, 1005–1010 (2008).



Extended Data Figure 1: Gel electrophoresis analysis of DNA brick cuboids. Structures were assembled isothermally for 5 – 7 days at the temperatures indicated above the lane. The label below a band of interest indicates the gel yield.



Extended Data Figure 2: Characterization of 30H \times 30H \times 260B cavity shapes. **a**, Schematic depicting the 30H \times 30H \times 260B molecular canvas in gray compared with a DNA origami-sized structure in blue. **b**, For each structure, the top panels show the 3D models of the designed structure. The bottom left panels shows expected TEM projections. The bottom right panels shows TEM averages from at least six particles. **c**, The structures were folded with 5 nM/strand by annealing isothermally or using a narrow ramp from 52.5 to 51°C. Products were analyzed on a 0.5% agarose gel in the presence of 10 mM MgCl₂. The percentage number listed below a target band indicates the gel yield. Lane labels correspond to those in Fig. 3 and in **(b)**.